

Electronic and dynamical properties of CeRh₂As₂: Role of Rh₂As₂ layers and expected hidden orbital order

Andrzej Ptok,^{1,*} Konrad J. Kapcia,² Paweł T. Jochym,¹
Jan Łażewski,¹ Andrzej M. Oleś,^{3,4} and Przemysław Piekarczyk^{1,†}

¹*Institute of Nuclear Physics, Polish Academy of Sciences, W. E. Radzikowskiego 152, PL-31342 Kraków, Poland*

²*Faculty of Physics, Adam Mickiewicz University in Poznań, Uniwersytetu Poznańskiego 2, PL-61614 Poznań, Poland*

³*Institute of Theoretical Physics, Jagiellonian University, Profesora Stanisława Łojasiewicza 11, PL-30348 Kraków, Poland*

⁴*Max Planck Institute for Solid State Research, Heisenbergstrasse 1, D-70569 Stuttgart, Germany*

(Dated: April 23, 2021)

Recently discovered heavy fermion CeRh₂As₂ compound crystallizes in the nonsymmorphic $P4/nmm$ symmetry, which enables the occurrence of topological protection. Experimental results show that this material exhibits unusual behavior, which is manifested by the appearance of two superconducting phases. In this work, we uncover and discuss a role of Rh₂As₂ layers and their impact on the electronic and dynamical properties of the system. The location of Ce atoms between two non-equivalent layers allows for the realization of hidden orbital order. We point out that the electronic band structure around the Fermi level is associated mostly with Ce 4*f* and Rh 4*d* orbitals and suggest the occurrence of the Lifshitz transition induced by the external magnetic field. We discuss also the role played by the *f*-*d* orbital hybridization in the electronic band structure.

Introduction. — Recently discovered CeRh₂As₂ superconductor [1] is one of rare examples of a heavy fermion systems crystallizing in $P4/nmm$ space group. In contrast to isostructural SrPt₂As₂ [2] or RPt₂Si₂ (where *R*=Y, La, Nd, and Lu) [3], it does not exhibit the coexistence of superconductivity and charge density waves.

In the case of CeRh₂As₂, two anomalies in the specific heat are observed below 1 K [1]. First anomaly (at lower temperature) is associated with the phase transition from the normal state to the superconducting (SC) phase (connected with a diamagnetic drop of the ac-susceptibility and the specific heat jump of the same order of magnitude as the Bardeen–Cooper–Schrieffer value). Second anomaly (at higher temperature) is not associated with superconductivity, but likely signals some other kind of order (its *T_c* increases with the in-plane magnetic field). In the presence of the magnetic field perpendicular to the Rh₂As₂ layers, the system exhibits a phase transition inside the SC state. It is suggested that at the transition the parity of superconductivity changes from even to odd one. This leads to *H-T* phase diagram in a characteristic form [1], which can be treated as a generic one for a realization of spin-singlet and spin-triplet SC phases [4]. Here, we would like to emphasize that this behavior is also observed in other systems, where a coexistence of trivial and topological SC phases can occur [5–7] due to finite spin-orbit coupling (SOC), whereas the ranges, in which both kinds of superconductivity exist strongly depend on model parameters, e.g. on the ratio of electron hopping and SOC [8].

The symmetry of the system described by $P4/nmm$ space group is nonsymmorphic with multiple symmetries protecting the Dirac points [9]. The similar situation has been recently reported for Dirac semimetals, crystallizing in the same symmetry [10–16]. However, contrary to these materials, where a dominant role is played by the

square nets [17], in the CeRh₂As₂ compound, there exist two different types of Rh₂As₂ layers (Fig. 1). What is more important, these layers can be treated as planes of the glide symmetry. The purpose of this Letter is to highlight the important role played by the Rh₂As₂ layers in possible realization of the hidden orbital order as a result of two distinguishable Ce atom positions with respect to the neighboring Rh₂As₂ layers. We point out that an existence of this order leads to essential modification of the phonon dispersion and could be tested by experimental measurements. We discuss also possibility of the Lifshitz transition induced by the magnetic field as a source of the topological superconducting phase reported experimentally in Ref. [1].

The density functional theory (DFT) calculations were performed using the VASP code [18–20]. Phonon calculations were conducted by ALAMODE [21] for the thermal distribution of multi-displacement of atoms at *T* = 50 K, generated within the HECSS procedure [22]. More details

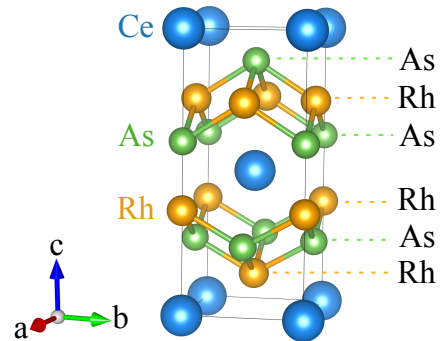


FIG. 1. The unit cell of the CeRh₂As₂ crystal structure. The system is composed of two Rh₂As₂ layers, which separately play a role of the mirrors of the glide symmetry.

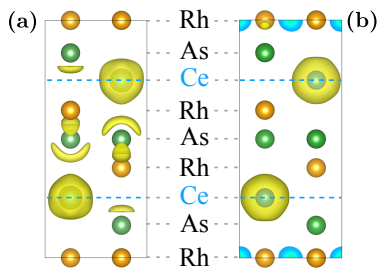


FIG. 2. (a) The electron localization function and (b) the partial charge density (for occupied states 1 eV below the Fermi level) in CeRh_2As_2 . Results were obtained in the presence of SOC and with Ce $4f$ electrons treated as valence electrons.

of numerical calculation can be found in Refs. [23–26] and in the Supplemental Material (SM) [27].

Crystal structure. — CeRh_2As_2 crystallizes in the CaBe_2Ge_2 [28] tetragonal structure (with symmetry $P4/nmm$, space group no. 129). The stacking sequence along c -axis is $\text{Ce-Rh}_2\text{As}_2\text{-Ce-Rh}_2\text{As}_2\text{-Ce}$, in which Rh_2As_2 layers are arranged in two non-equivalent forms: square array of Rh atoms sandwiched between two checkerboard layers of As atoms (one below and one above the Rh layer, alternately) and *vice versa* (square As layer decorated by Rh atoms, alternately, from top and bottom). This corresponds to upper and lower Rh_2As_2 layers in Fig. 1.

The unit cell of the studied system consists of two formula units. From the *ab initio* calculations (with the PBEsol pseudopotentials, see SM [27]), we find the lattice constants as $a = 4.2216 \text{ \AA}$ and $c = 9.8565 \text{ \AA}$, which are in good agreement with the experimental results [1]. In the case of Ce $4f$ electrons treated as valence electrons, the ground state (GS) of the system is found to be nonmagnetic (cf. the SM [27]).

Glide symmetry. — The nonsymmorphic space group of CeRh_2As_2 , unusual for heavy fermion systems [29, 30], supports realization of the unconventional SC gap in the electronic structure [31] protected by the space group symmetry [32]. This space group exhibits the glide symmetry, which is here realized by the Rh and As square nets inside Rh_2As_2 layers. Therefore, orbitals of Ce atoms should also exhibit the glide symmetry with respect to these planes. Simultaneously, the Ce electron orbitals lose the mirror symmetry (along c -direction) due to different environments from “top” and “bottom” sides (cf. Fig. 1). Indeed, this behavior is clearly manifested directly via the electron localization function [33–35] [Fig. 2(a)] or partial charge density [Fig. 2(b)]. As one can see in Fig. 2(a), localization of electrons around Ce atom (at the center of the system) does not exhibit symmetry with respect to the ab plane (marked by dashed blue line). Similar property is observed in the case of partial charge density coming from occupied

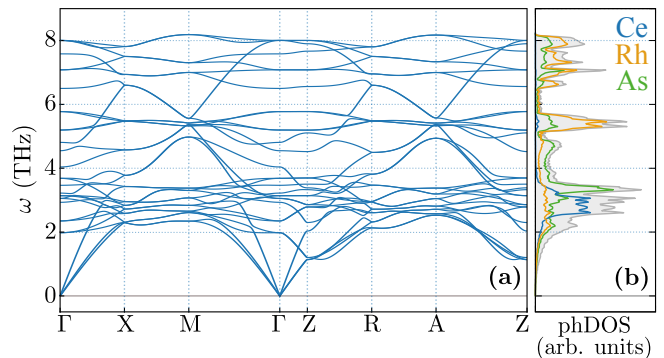


FIG. 3. Results of phonon calculations in CeRh_2As_2 : (a) phonon dispersion curves along high-symmetry directions; (b) total and partial phonon DOSs, shown by gray and color (as labeled) solid lines, respectively. Results were obtained in the presence of SOC and with Ce $4f$ electrons treated as valence electrons.

states around the Fermi level (we take states 1 eV below the Fermi level). In consequence, both Ce atoms of the unit cell are distinguishable due to relative position with respect to Rh_2As_2 layers and effectively realized pseudo-orbitals. This scenario is remarkably similar to URu_2Si_2 [36], where the orbitals located at U atoms exhibit out-of-plane anisotropy and the ground state is discussed as a superposition of different irreducible representations [37] resulting in the crystal-field states [38], and thus we suggest that the orbital order can be called *hidden orbital order*.

In our case, hidden orbital order can occur due to broken reflection symmetry at Ce atoms. The onset of hidden order in CeRh_2As_2 associated with the symmetry breaking at the Ce sites could lower the symmetry from $P4/nmm$ (space group no. 129) to $P4mm$ (space group no. 99). The similar effect of symmetry lowering can be achieved by introducing antiferromagnetic order on the sublattice of Ce atoms. This can be crucial in context of the realization of the non-trivial topological phase, due to fact that the information about the non-trivial phase realization can be attained from the number of the bands crossing the Fermi level [39]. Changed degeneracy of the bands by symmetry modifications can lead to a different topological phase realized in the system. However, because the band structure is relatively dense and a few bands have the maxima located around the Fermi level, the results obtained in this way can be ambiguous.

Lattice dynamics. — The phonon dispersion curves and DOSs are shown in Fig. 3. As one can see, CeRh_2As_2 is stable dynamically, i.e., the soft modes (imaginary frequencies) are not observed. The irreducible representations at the the Γ point are: $E_u + A_{2u}$ for acoustic modes, and $4E_u + 4A_{2u} + 5E_g + 3A_{1g} + 2B_{1g}$ for optic modes.

Partial DOSs clearly show that the modes associated with Ce atoms are located mostly at lower frequencies in a range of $2 \div 3 \text{ THz}$. This is a typical behavior ob-

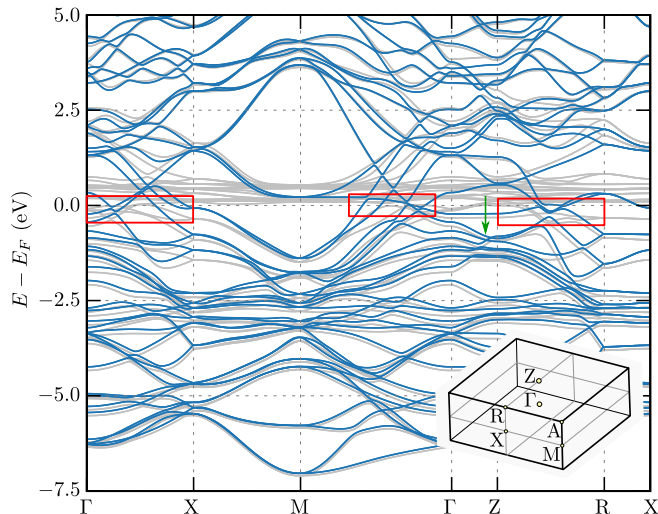


FIG. 4. Electronic band structures of CeRh_2As_2 in the presence of the SOC. Solid blue and gray lines correspond to different treatments of the Ce $4f$ electrons (as core and as valence electrons, respectively).

served in clathrates [40], when some heavy atoms are located inside a “cage”. In our case, Ce is located inside cage-like dodecahedron constructed by two Rh_2As_2 layers (cf. Fig. 1). Indeed, similar behavior is observed e.g. in the case of KFe_2As_2 [41] with I_4/mmm symmetry. There, the modes involving K atom located between Fe_2Se_2 layers are observed only at lower frequencies [Fig. 3(b)]. Such situation leads to the emergence of nearly flat phonon bands with weak contribution to lattice thermal conductivity, due to small group velocity and short phonon life-time. Moreover, this physical behavior can be examined experimentally by the phonon life-time measurements [42]. One finds that modes mixing vibrations of Rh and As atoms are of particular interest and are visible in the whole range of phonon spectrum.

The effect of hidden orbital order on phonon spectra is noticeable by comparing the results for the P_4/nmm and P_4mm space groups (without and with orbital order, respectively). By reducing symmetry, we find small shift of energies and splitting of phonon branches resulting from slightly different charge distribution on two sites of Ce atoms (Fig. S1 in the SM [27]). This effect could be verified in the future by the inelastic scattering measurements [43–45].

Electronic band structure. — Calculated electronic band structure in the presence of SOC is presented in Fig. 4. The absence of magnetic order in CeRh_2As_2 leads to spin degeneracy of electronic bands in the P_4/nmm symmetry. For instance, at $k_z = 0$ the degeneracy of the bands is preserved at the X and M points. Additionally, along the Γ –Z direction the bands cross below the Fermi level (marked by the green arrow in Fig. 4). Similar behavior is observed in the nonmagnetic Dirac semimetals

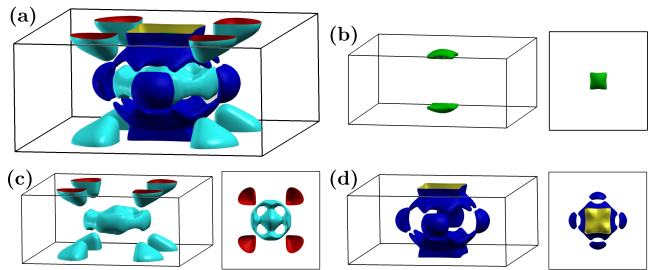


FIG. 5. (a) The Fermi surface of CeRh_2As_2 and (b)–(d) its separate pockets (side and top views). Results were obtained in the presence of SOC and for Ce $4f$ electrons treated as valence electrons.

(with the same symmetry), like in CeSbTe [14]. However, note that the Dirac point and non-trivial topology can be expected even in canonical heavy fermion systems like CeCoIn_5 [46] with the P_4/mmm symmetry.

CeRh_2As_2 can be compared with SrPt_2As_2 [47, 48] and LaPt_2Si_2 [48], both crystallizing in the same P_4/nmm symmetry. The SOC has weaker impact on the band structure of CeRh_2As_2 than for SrPt_2As_2 [47, 48] and is comparable with the impact on the band structure of LaPt_2Si_2 [48] (cf. Fig. S4 in the SM [27]). These changes can be a consequence of the modifications of chemical composition, due to the mass dependence of the SOC [49, 50]. Indeed, the biggest splitting of the bands induced by the SOC is well visible in the unoccupied Ce $4f$ energy levels (around $0.25 \div 0.5$ eV above the Fermi level).

The band structure shows the shift of the Fermi level in CeRh_2As_2 to lower energies w.r.t. SrPt_2As_2 [47, 48] and LaPt_2Si_2 [48]. In both latter compounds, the band structures around the Fermi level are associated with the atoms located in layers, i.e., Pt and As in SrPt_2As_2 [47, 48], as well as Pt and Si in LaPt_2Si_2 [48]. In our case, the band structure around the Fermi level originates mostly from Ce $4f$ and Rh $4d$ electrons, what is well visible on the orbital projection of bands (see Fig. S3 in SM [27]). The Ce $4f$ electrons are located at relatively small range of energies, what leads to well visible peak of the density of states (see Fig. S2 in SM [27]). However, the Rh_2As_2 layers play important role in the general form of the band structure in CeRh_2As_2 . This is well visible when we compare the band structure of real CeRh_2As_2 with an artificial system without Ce atoms (i.e., containing only two Rh_2As_2 layers), cf. Fig. S5 in the SM [27]. The main features of the artificial Rh_2As_2 system are conserved and well visible in the band structure of CeRh_2As_2 . The differences arise only from $5d$ electron levels of Ce atoms occupied by one electron.

Fermi surface. — The Fermi surface of CeRh_2As_2 [Fig. 5(a)] is composed of three pockets [see Figs. 5(b)–5(d)], which exhibit three dimensional (3D) character. Contrary to the other heavy fermion systems, e.g. to CeCoIn_5 [51–57], there is no pocket with quasi-two di-

mensional features (i.e., no pockets with weak z -direction dependence). Theoretical calculations of the electronic structure show that the band structure around the Fermi level can be very sensitive to chemical doping [see red boxes in Fig. 4]. This is associated with relatively large number of hybridized bands. Similarly, the external magnetic field can lead to meaningful modification of the electronic structure, as well as of the character of the Fermi pockets.

Role of 4f electrons. — Comparison of the band structures, when Ce 4f electrons are treated as core or valence electrons in the DFT calculations, are shown in Fig. 4 (solid blue and gray lines, respectively). The Ce 4f electrons energy levels are located around 0.25 eV and 0.5 eV above the Fermi level, due to the relatively strong SOC [58]. The f - d orbital hybridization leads to modification of the band structure around the Fermi level. In practice, all energy levels are slightly shifted to lower energies, while band characters are almost unchanged [cf. grey and blue lines on Fig. 4].

Similarly like in the other heavy fermion systems with I_4/mmm symmetry (such as, e.g., URu₂Si₂ [59], CeRh₂Si₂ [60, 61], YbIr₂Si₂/YbRh₂Si₂ [62, 63], or EuRh₂Si₂ [64–66]), the f - d orbital hybridization can play important role. Indeed, orbital projected band structure show strong impact of the Ce 4f and Rh 4d orbitals onto states around the Fermi level (see Fig. S3 in the SM [27]). This behavior can be important in the context of the correct theoretical description of studied system and can be indescribable within the simple tight-binding model formulation [1, 4, 8, 67]. Nevertheless, the exact form of the electronic band structure around the Fermi level should be examined by the future investigations within the high quality angle-resolved photoemission spectroscopy (ARPES) measurements [68–70].

The lattice constants found in the numerical calculations depend on the description of 4f electrons of Ce atoms (cf. Tables S1–S4 in the SM [27]). Better agreement of numerical results with experimental data is obtained when the 4f electrons are treated as valence electrons. This behavior is well known and associated with the formation of stronger bonding in systems including f electrons, what leads to a decreased volume.

Magnetic instability. — The GS found from the *ab initio* calculations is nonmagnetic. However, Ce atoms have non-zero magnetic moments of magnitude below 0.03 μ_B . This can be a symptom of magnetic instability of the system, which could lead to magnetic ordering at lower temperatures. Regardless of the GS, the numerical calculations with initially enforced different magnetic orders uncover structures with lattice constants better matching experimental values (cf. Tab. S3 in the SM [27]). These enforced initial magnetic orders can discriminate between two Ce atomic sites and support the realization of previously mentioned hidden orbital order. However, this case is out of the scope of this work and

should be studied in the future.

Lifshitz transition. — We emphasize that several bands are located close to the Fermi level. Here, one should particularly point out the bands with maxima or minima around the Fermi level, i.e., bands inside red boxes in Fig. 4. External magnetic field, due to the Zeeman effect and band splitting, can lead to emergence of a new, fully polarized Fermi pocket, or to disappearance of the existing one. This phenomenon, called *magnetic Lifshitz transition* (MLT), was described in the context of high-magnetic field phase observed in FeSe [71]. During the MLT the modification of the Fermi surface topology is observed, which could be realized here by the external magnetic field [71, 72].

To mimic a tendency of CeRh₂As₂ to the realization of MLT, we performed calculations with non-equal number of spin-up and spin-down electrons, i.e., in a spin-polarized state (cf. Fig. S6 in the SM [27]). For a comparison, we calculated band structures for several values of the spin imbalance. In such a case, we notice two effects: (i) the artificially introduced polarization changes the Fermi level, and (ii) strong modifications of the Fermi pockets even by small change of the Fermi level (cf. Fig. S7 in the SM [27]). For example, the smallest Fermi pocket [presented on Fig. 5(b)] can disappear as a result of a shift of the Fermi level by 0.01 eV.

Finally, note that the mentioned shift of the Fermi level by 0.01 eV corresponds to relatively large external magnetic field. However, one expects that the arising magnetic order may in turn induce sufficient internal “effective” magnetic field. This resembles the antiferromagnetic-like order in other heavy fermion compounds (in the presence of the external magnetic field). As an example one can mention here the Q -phase in CeCoIn₅ [73–75]. We underline that the magnetic field, at which the MLT occurs, has approximately constant value [71, 72, 76]. Experimentally, the transition observed in CeRh₂As₂ occurs also at approximately constant magnetic field [1].

The realization of the MLT can change the topological character of CeRh₂As₂. Similarly to mentioned before case of orbital order, the change in degeneracy or the number of bands crossing directly the Fermi level, can change the topological character of the system. Indeed, this behavior can be shown by theoretical calculation based on the tight-binding model [67]. In such situation, the realization of the topological surface edge state is expected, what makes this material interesting also in a context of topological properties or applications.

Conclusions. — Summarizing, by using the *ab initio* techniques we investigated the physical properties of the CeRh₂As₂ compound. The specific crystal structure as well as the previous investigations on heavy fermion compounds with the same $P4/nmm$ symmetry suggest a prominent role of the Rh₂As₂ layers in the properties of this compound. Their impact is visible in the

phonon spectra, where Ce modes are located only at lower frequencies due to the cage-like structure built by Rh_2As_2 layers. Additionally, orbital projections of electronic band structure suggest the strong hybridization between Ce $4f$ and Rh $4d$ electrons. The electronic states located around the Fermi level are mostly composed by orbitals of these types, what may be important for construction of a realistic tight binding model of this compound.

Due to location of Ce atoms between two nonequivalent Rh_2As_2 layers the emergence of the hidden orbital ordering is supported. As a result, two distinguishable Ce sublattices with different effective “orbitals” are found. Similarly as in URu_2As_2 , such orbitals exhibit out-of-plane anisotropy. This orbital order should occur independently of the external magnetic field. Moreover, in practice, this orbital order leads to lowering of the system symmetry. As a consequence, the measurable modifications of the phonon band degeneracy occur.

From the observed small band splitting we conclude that the spin-orbit coupling is relatively weak. However, the electronic band structure of CeRh_2As_2 reveals specific topological properties of this system. First, we can observe band crossing (the Dirac points), approximately 1 eV below the Fermi level. Second, the bands near the Fermi level support the hypothesis of the magnetic Lifshitz transition. At finite magnetic field, the new fully polarized Fermi pocket could emerge, and the spin-triplet pairing (topological superconducting phase) would arise.

We warmly thank Dominik Legut for insightful discussions. Some figures in this work were rendered using VESTA [77] and XCRYSDEN [78] software. This work was supported by National Science Centre (NCN, Poland) under Projects 2016/21/D/ST3/03385 (A.P.), 2017/24/C/ST3/00276 (K.J.K.), 2016/23/B/ST3/00839 (A.M.O.), and 2017/25/B/ST3/02586 (P.P.). In addition, A.P. and K.J.K. are grateful for the funding from the scholarships of the Minister of Science and Higher Education (Poland) for outstanding young scientists (2019 edition, Nos. 818/STYP/14/2019 and 821/STYP/14/2019, respectively).

* e-mail: aptok@mmj.pl

† e-mail: piekarz@wolf.ifj.edu.pl

- [1] S. Khim, J. F. Landaeta, J. Banda, N. Bannor, M. Brando, P. M. R. Brydon, D. Hafner, R. Küchler, R. Cardoso-Gil, U. Stockert, A. P. Mackenzie, D. F. Agterberg, C. Geibel, and E. Hassinger, “Field-induced transition from even to odd parity superconductivity in CeRh_2As_2 ,” (2021), [arXiv:2101.09522](https://arxiv.org/abs/2101.09522).
- [2] K. Kudo, Y. Nishikubo, and M. Nohara, “Coexistence of superconductivity and charge density wave in SrPt_2As_2 ,” *J. Phys. Soc. Jpn.* **79**, 123710 (2010).
- [3] Y. Nagano, N. Araoka, A. Mitsuda, H. Yayama, H. Wada, M. Ichihara, M. Isobe, and Y. Ueda, “Charge density wave and superconductivity of RPt_2Si_2 ($R = \text{Y, La, Nd, and Lu}$),” *J. Phys. Soc. Jpn.* **82**, 064715 (2013).
- [4] E. G. Schertenleib, M. H. Fischer, and M. Sigrist, “Unusual H - T phase diagram of CeRh_2As_2 – the role of staggered non-centrosymmetry,” (2021), [arXiv:2101.08821](https://arxiv.org/abs/2101.08821).
- [5] T. Yoshida, M. Sigrist, and Y. Yanase, “Parity-mixed superconductivity in locally non-centrosymmetric system,” *J. Phys. Soc. Jpn.* **83**, 013703 (2014).
- [6] D. Möckli and M. Khodas, “Robust parity-mixed superconductivity in disordered monolayer transition metal dichalcogenides,” *Phys. Rev. B* **98**, 144518 (2018).
- [7] D. Möckli and M. Khodas, “Magnetic-field induced $s + if$ pairing in Ising superconductors,” *Phys. Rev. B* **99**, 180505(R) (2019).
- [8] D. Möckli and A. Ramires, “Two scenarios for superconductivity in CeRh_2As_2 ,” (2021), [arXiv:2102.09425](https://arxiv.org/abs/2102.09425).
- [9] S. M. Young and C. L. Kane, “Dirac semimetals in two dimensions,” *Phys. Rev. Lett.* **115**, 126803 (2015).
- [10] L. M. Schoop, M. N. Ali, C. Straßer, A. Topp, A. Varykhalov, D. Marchenko, V. Duppel, S. S. P. Parkin, B. V. Lotsch, and Ch. R. Ast, “Dirac cone protected by non-symmorphic symmetry and three-dimensional Dirac line node in ZrSiS ,” *Nat. Commun.* **7**, 11696 (2016).
- [11] D. Takane, Zhiwei Wang, S. Souma, K. Nakayama, C. X. Trang, T. Sato, T. Takahashi, and Yoichi Ando, “Dirac-node arc in the topological line-node semimetal HfSiS ,” *Phys. Rev. B* **94**, 121108(R) (2016).
- [12] M. M. Hosen, K. Dimitri, I. Belopolski, P. Maldonado, R. Sankar, N. Dhakal, G. Dhakal, T. Cole, P. M. Oppeneer, D. Kaczorowski, F. Chou, M. Z. Hasan, T. Durakiewicz, and M. Neupane, “Tunability of the topological nodal-line semimetal phase in ZrSiX -type materials ($X = \text{S, Se, Te}$),” *Phys. Rev. B* **95**, 161101(R) (2017).
- [13] C. Chen, X. Xu, J. Jiang, S.-C. Wu, Y. P. Qi, L. X. Yang, M. X. Wang, Y. Sun, N. B. M. Schröter, H. F. Yang, L. M. Schoop, Y. Y. Lv, J. Zhou, Y. B. Chen, S. H. Yao, M. H. Lu, Y. F. Chen, C. Felser, B. H. Yan, Z. K. Liu, and Y. L. Chen, “Dirac line nodes and effect of spin-orbit coupling in the nonsymmorphic critical semimetals $M\text{SiS}$ ($M = \text{Hf, Zr}$),” *Phys. Rev. B* **95**, 125126 (2017).
- [14] L. M. Schoop, A. Topp, J. Lippmann, F. Orlandi, L. Mühler, M. G. Vergniory, Y. Sun, A. W. Rost, V. Duppel, M. Krivenkov, S. Sheoran, P. Manuel, A. Varykhalov, B. Yan, R. K. Kremer, Ch. R. Ast, and B. V. Lotsch, “Tunable Weyl and Dirac states in the non-symmorphic compound CeSbTe ,” *Sci. Adv.* **4**, eaar2317 (2018).
- [15] S. Pezzini, M. R. van Delft, L. M. Schoop, B. V. Lotsch, A. Carrington, M. I. Katsnelson, N. E. Hussey, and S. Wiedmann, “Unconventional mass enhancement around the Dirac nodal loop in ZrSiS ,” *Nat. Phys.* **14**, 178 (2018).
- [16] Y.-Y. Wang, S. Xu, L.-L. Sun, and T.-L. Xia, “Quantum oscillations and coherent interlayer transport in a new topological dirac semimetal candidate YbMnSb_2 ,” *Phys. Rev. Materials* **2**, 021201(R) (2018).
- [17] S. Klemenz, S. Lei, and L. M. Schoop, “Topological semimetals in square-net materials,” *Annu. Rev. Mater. Res.* **49**, 185 (2019).
- [18] G. Kresse and J. Hafner, “Ab initio molecular-dynamics simulation of the liquid-metal-amorphous-semiconductor transition in germanium,” *Phys. Rev. B* **49**, 14251 (1994).

- [19] G. Kresse and J. Furthmüller, “Efficient iterative schemes for ab initio total-energy calculations using a plane-wave basis set,” *Phys. Rev. B* **54**, 11169 (1996).
- [20] G. Kresse and D. Joubert, “From ultrasoft pseudopotentials to the projector augmented-wave method,” *Phys. Rev. B* **59**, 1758 (1999).
- [21] T. Tadano, Y. Gohda, and S. Tsuneyuki, “Anharmonic force constants extracted from first-principles molecular dynamics: applications to heat transfer simulations,” *J. Phys.: Condens. Matter* **26**, 225402 (2014).
- [22] P. T. Jochym and J. Łażewski, “High Efficiency Configuration Space Sampling – probing the distribution of available states,” (2021), SciPost Physics: scipost_202101.00011v1 (submission).
- [23] P. E. Blöchl, “Projector augmented-wave method,” *Phys. Rev. B* **50**, 17953 (1994).
- [24] J. P. Perdew, K. Burke, and M. Ernzerhof, “Generalized gradient approximation made simple,” *Phys. Rev. Lett.* **77**, 3865 (1996).
- [25] J. P. Perdew, A. Ruzsinszky, G. I. Csonka, O. A. Vydrov, G. E. Scuseria, L. A. Constantin, X. Zhou, and K. Burke, “Restoring the density-gradient expansion for exchange in solids and surfaces,” *Phys. Rev. Lett.* **100**, 136406 (2008).
- [26] H. J. Monkhorst and J. D. Pack, “Special points for Brillouin-zone integrations,” *Phys. Rev. B* **13**, 5188 (1976).
- [27] See the Supplemental Material at [URL will be inserted by publisher] for the description of numerical methods details, additional numerical results discussing: lattice constants, band structure, phonons spectra and Lifshitz transition.
- [28] Q. G. Mu, B. J. Pan, B. B. Ruan, T. Liu, K. Zhao, L. Shan, G. F. Chen, and Z. A. Ren, “Superconductivity in LaPd₂Bi₂ with CaBe₂Ge₂-type structure,” *Sci. China Phys. Mech. Astron.* **61**, 127409 (2018).
- [29] E. M. Nica, R. Yu, and Q. Si, “Glide reflection symmetry, Brillouin zone folding, and superconducting pairing for the $P4/nmm$ space group,” *Phys. Rev. B* **92**, 174520 (2015).
- [30] R. Nourafkan and A.-M. S. Tremblay, “Effect of nonsymorphic space groups on correlation functions in iron-based superconductors,” *Phys. Rev. B* **96**, 125140 (2017).
- [31] V. Cvetkovic and O. Vafek, “Space group symmetry, spin-orbit coupling, and the low-energy effective Hamiltonian for iron-based superconductors,” *Phys. Rev. B* **88**, 134510 (2013).
- [32] S. Sumita and Y. Yanase, “Unconventional superconducting gap structure protected by space group symmetry,” *Phys. Rev. B* **97**, 134512 (2018).
- [33] A. D. Becke and K. E. Edgecombe, “A simple measure of electron localization in atomic and molecular systems,” *J. Chem. Phys.* **92**, 5397 (1990).
- [34] A. Savin, O. Jepsen, J. Flad, O. K. Andersen, H. Preuss, and H. G. von Schnering, “Electron localization in solid-state structures of the elements: the diamond structure,” *Angew. Chem., Int. Ed. Engl.* **31**, 187 (1992).
- [35] B. Silvi and A. Savin, “Classification of chemical bonds based on topological analysis of electron localization functions,” *Nature* **371**, 683 (1994).
- [36] P. Chandra, P. Coleman, J. A. Mydosh, and V. Tripathi, “Hidden orbital order in the heavy fermion metal URu₂Si₂,” *Nature* **417**, 831 (2002).
- [37] M. Sundermann, M. W. Haverkort, S. Agrestini, A. Al-Zein, M. Moretti Sala, Y. Huang, M. Golden, A. de Visser, P. Thalmeier, L. H. Tjeng, and A. Severing, “Direct bulk-sensitive probe of 5f symmetry in URu₂Si₂,” *Proc. Natl. Acad. Sci. U.S.A.* **113**, 13989–13994 (2016).
- [38] H.-H. Kung, R. E. Baumbach, E. D. Bauer, V. K. Thorsmølle, W.-L. Zhang, K. Haule, J. A. Mydosh, and G. Blumberg, “Chirality density wave of the “hidden order” phase in URu₂Si₂,” *Science* **347**, 1339 (2015).
- [39] M. Z. Hasan and C. L. Kane, “*Colloquium*: topological insulators,” *Rev. Mod. Phys.* **82**, 3045–3067 (2010).
- [40] T. Takabatake, K. Suekuni, T. Nakayama, and E. Kaneshita, “Phonon-glass electron-crystal thermoelectric clathrates: Experiments and theory,” *Rev. Mod. Phys.* **86**, 669 (2014).
- [41] A. Ptok, M. Sternik, K. J. Kapcia, and P. Piekarczyk, “Structural, electronic, and dynamical properties of the tetragonal and collapsed tetragonal phases of KFe₂As₂,” *Phys. Rev. B* **99**, 134103 (2019).
- [42] P.-F. Lory, S. Pailhès, V. M. Giordano, H. Euchner, H. D. Nguyen, R. Ramlau, H. Borrmann, M. Schmidt, M. Baitinger, M. Ikeda, P. Tomáš, M. Mihalkovič, C. Allio, M. R. Johnson, H. Schober, Y. Sidis, F. Bourdarot, L. P. Regnault, J. Ollivier, S. Paschen, Y. Grin, and M. de Boissieu, “Direct measurement of individual phonon lifetimes in the clathrate compound Ba_{7.81}Ge_{40.67}Au_{5.33},” *Nat. Commun.* **8**, 491 (2017).
- [43] O. Delaire, J. Ma, K. Marty, A. F. May, M. A. McGuire, M.-H. Du, D. J. Singh, A. Podlesnyak, G. Ehlers, M. D. Lumsden, and B. C. Sales, “Giant anharmonic phonon scattering in PbTe,” *Nat. Mater.* **10**, 614 (2011).
- [44] J. Ma, O. Delaire, A. F. May, C. E. Carlton, M. A. McGuire, L. H. VanBebber, D. L. Abernathy, G. Ehlers, Tao Hong, A. Huq, Wei Tian, V. M. Keppens, Y. Shao-Horn, and B. C. Sales, “Glass-like phonon scattering from a spontaneous nanostructure in AgSbTe₂,” *Nat. Nanotech.* **8**, 445 (2013).
- [45] C. W. Li, J. Hong, A. F. May, D. Bansal, S. Chi, T. Hong, G. Ehlers, and O. Delaire, “Orbitally driven giant phonon anharmonicity in SnSe,” *Nat. Phys.* **11**, 1063 (2015).
- [46] K. R. Shirer, Y. Sun, M. D. Bachmann, C. Putzke, T. Helm, L. E. Winter, F. F. Balakirev, R. D. McDonald, J. G. Analytis, N. L. Nair, E. D. Bauer, F. Ronning, C. Felser, T. Meng, B. Yan, and P. J. W. Moll, “Dirac fermions in the heavy-fermion superconductors Ce(Co,Rh,Ir)In₅,” (2018), arXiv:1808.00403.
- [47] I. A. Nekrasov and M. V. Sadovskii, “Electronic structure of novel multiple-band superconductor SrPt₂As₂,” *JETP Letters* **92**, 751 (2010).
- [48] S. Kim, K. Kim, and B. I. Min, “The mechanism of charge density wave in Pt-based layered superconductors: SrPt₂As₂ and LaPt₂Si₂,” *Sci. Rep.* **5**, 15052 (2015).
- [49] F. Herman, Ch. D. Kuglin, K. F. Cuff, and R. L. Kortum, “Relativistic corrections to the band structure of tetrahedrally bonded semiconductors,” *Phys. Rev. Lett.* **11**, 541 (1963).
- [50] K. V. Shanavas, Z. S. Popović, and S. Satpathy, “Theoretical model for Rashba spin-orbit interaction in *d* electrons,” *Phys. Rev. B* **90**, 165108 (2014).
- [51] R. Settai, H. Shishido, S. Ikeda, Y. Murakawa, M. Nakashima, D. Aoki, Y. Haga, H. Harima, and Y. Onuki, “Quasi-two-dimensional fermi surfaces and the de Haas-van Alphen oscillation in both the normal and superconducting mixed states of CeCoIn₅,” *J. Phys.: Con-*

- dens. Matter **13**, L627 (2001).
- [52] H. Shishido, R. Settai, D. Aoki, Shugo Ikeda, H. Nakawaki, N. Nakamura, T. Iizuka, Y. Inada, K. Sugiyama, T. Takeuchi, K. Kindo, T. C. Kobayashi, Y. Haga, H. Harima, T. Aoki, Y. and Namiki, H. Sato, and Y. Onuki, “Fermi surface, magnetic and superconducting properties of LaRhIn_5 and CeTIn_5 (T : Co, Rh and Ir),” *J. Phys. Soc. Jpn.* **71**, 162 (2002).
- [53] T. Maehira, T. Hotta, K. Ueda, and A. Hasegawa, “Relativistic band-structure calculations for CeTIn_5 (T = Ir and Co) and analysis of the energy bands by using tight-binding method,” *J. Phys. Soc. Jpn.* **72**, 854 (2003).
- [54] P. M. Oppeneer, S. Elgazzar, A.B. Shick, I. Opahle, J. Ruzs, and R. Hayn, “Fermi surface changes due to localized–delocalized f -state transitions in Ce-115 and Pu-115 compounds,” *J. Magn. Magn. Mater.* **310**, 1684 (2007).
- [55] F. Ronning, J.-X. Zhu, T. Das, M. J. Graf, R. C. Albers, H. B. Rhee, and W. E. Pickett, “Superconducting gap structure of the 115s revisited,” *J. Phys.: Condens. Matter* **24**, 294206 (2012).
- [56] A. Polyakov, O. Ignatchik, B. Bergk, K. Götze, A. D. Bianchi, S. Blackburn, B. Prévost, G. Seyfarth, M. Côté, D. Hurt, C. Capan, Z. Fisk, R. G. Goodrich, I. Sheikin, Manuel Richter, and J. Wosnitza, “Fermi-surface evolution in Yb-substituted CeCoIn_5 ,” *Phys. Rev. B* **85**, 245119 (2012).
- [57] A. Ptok, K. J. Kapcia, P. Piekarz, and A. M Oleś, “The ab initio study of unconventional superconductivity in CeCoIn_5 and FeSe ,” *New J. Phys.* **19**, 063039 (2017).
- [58] We also compared the electronic band structure from VASP with results obtained within QUANTUM ESPRESSO software [79, 80] and pseudopotentials developed in a frame of PSLIBRARY [81]. One needs to notice that the Ce atoms in both cases have different electronic configuration, i.e., $[\text{Xe}] 6s^2 4f^{0.5} 5d^{1.5}$ in the case PSLIBRARY and $[\text{Xe}] 6s^2 4f^1 5d^1$ for VASP pseudopotentials. In consequence, the Ce $4f$ electrons levels can be overestimated (cf. Fig. 4 and Fig. S8 in SM [27]).
- [59] H. Ikeda, M.-T. Suzuki, R. Arita, and T. Takimoto, “Multipole fluctuations of itinerant f electrons and triakontadipole order in URu_2Si_2 ,” *Comptes Rendus Physique* **15**, 587 (2014).
- [60] S. Patil, A. Generalov, M. Güttler, P. Kushwaha, A. Chikina, K. Kummer, T. C. Rödel, A. F. Santander-Syro, N. Caroca-Canales, C. Geibel, S. Danzenbächer, Yu. Kucherenko, C. Laubschat, J. W. Allen, and D. V. Vyalikh, “ARPES view on surface and bulk hybridization phenomena in the antiferromagnetic kondo lattice CeRh_2Si_2 ,” *Nat. Commun.* **7**, 11029 (2016).
- [61] G. Poelchen, S. Schulz, M. Mende, M. Güttler, A. Generalov, A. V. Fedorov, N. Caroca-Canales, Ch. Geibel, K. Kliemt, C. Krellner, S. Danzenbächer, D. Y. Usachov, P. Dudin, V. N. Antonov, J. W. Allen, C. Laubschat, K. Kummer, Y. Kucherenko, and Denis V. Vyalikh, “Unexpected differences between surface and bulk spectroscopic and implied Kondo properties of heavy fermion CeRh_2Si_2 ,” *npj Quantum Mater.* **5**, 70 (2020).
- [62] S. Danzenbächer, Yu. Kucherenko, D. V. Vyalikh, M. Holder, C. Laubschat, A. N. Yaresko, C. Krellner, Z. Hossain, C. Geibel, X. J. Zhou, W. L. Yang, N. Manella, Z. Hussain, Z.-X. Shen, M. Shi, L. Patthey, and S. L. Molodtsov, “Momentum dependence of $4f$ hybridization in heavy-fermion compounds: Angle-resolved photoemission study of YbIr_2Si_2 and YbRh_2Si_2 ,” *Phys. Rev. B* **75**, 045109 (2007).
- [63] D. V. Vyalikh, S. Danzenbächer, Yu. Kucherenko, K. Kummer, C. Krellner, C. Geibel, M. G. Holder, T. K. Kim, C. Laubschat, M. Shi, L. Patthey, R. Follath, and S. L. Molodtsov, “ k dependence of the crystal-field splittings of $4f$ states in rare-earth systems,” *Phys. Rev. Lett.* **105**, 237601 (2010).
- [64] M. Höppner, S. Seiro, A. Chikina, A. Fedorov, M. Güttler, S. Danzenbächer, A. Generalov, K. Kummer, S. Patil, S. L. Molodtsov, Y. Kucherenko, C. Geibel, V. N. Strocov, M. Shi, M. Radovic, T. Schmitt, C. Laubschat, and D. V. Vyalikh, “Interplay of Dirac fermions and heavy quasiparticles in solids,” *Nat. Commun.* **4**, 1646 (2013).
- [65] A. Chikina, M. Höppner, S. Seiro, K. Kummer, S. Danzenbächer, S. Patil, A. Generalov, M. Güttler, Yu. Kucherenko, E. V. Chulkov, Yu. M. Koroteev, K. Koepf, C. Geibel, M. Shi, M. Radovic, C. Laubschat, and D. V. Vyalikh, “Strong ferromagnetism at the surface of an antiferromagnet caused by buried magnetic moments,” *Nat. Commun.* **5**, 3171 (2014).
- [66] M. Güttler, A. Generalov, S. I. Fujimori, K. Kummer, A. Chikina, S. Seiro, S. Danzenbächer, Yu. M. Koroteev, E. V. Chulkov, M. Radovic, M. Shi, N. C. Plumb, C. Laubschat, J. W. Allen, C. Krellner, C. Geibel, and D. V. Vyalikh, “Divalent EuRh_2Si_2 as a reference for the luttinger theorem and antiferromagnetism in trivalent heavy-fermion YbRh_2Si_2 ,” *Nat. Commun.* **10**, 796 (2019).
- [67] K. Nogaki, A. Daido, J. Ishizuka, and Y. Yanase, “Topological crystalline superconductivity in locally noncentrosymmetric CeRh_2As_2 ,” (2021), [arXiv:2103.08088](https://arxiv.org/abs/2103.08088).
- [68] A. Damascelli, Z. Hussain, and Z.-X. Shen, “Angle-resolved photoemission studies of the cuprate superconductors,” *Rev. Mod. Phys.* **75**, 473 (2003).
- [69] J Hugo Dil, “Spin and angle resolved photoemission on non-magnetic low-dimensional systems,” *J. Phys.: Condens. Matter* **21**, 403001 (2009).
- [70] Baiqing Lv, Tian Qian, and Hong Ding, “Angle-resolved photoemission spectroscopy and its application to topological materials,” *Nat. Rev. Phys.* **1**, 609 (2019).
- [71] A. Ptok, K. J. Kapcia, A. Cichy, A. M. Oleś, and P. Piekarz, “Magnetic Lifshitz transition and its consequences in multi-band iron-based superconductors,” *Sci. Rep.* **7**, 41979 (2017).
- [72] R. Daou, C. Bergemann, and S. R. Julian, “Continuous evolution of the Fermi surface of CeRu_2Si_2 across the metamagnetic transition,” *Phys. Rev. Lett.* **96**, 026401 (2006).
- [73] M. Kenzelmann, Th. Strässle, C. Niedermayer, M. Sigrist, B. Padmanabhan, M. Zolliker, A. D. Bianchi, R. Movshovich, E. D. Bauer, J. L. Sarrao, and J. D. Thompson, “Coupled superconducting and magnetic order in CeCoIn_5 ,” *Science* **321**, 1652 (2008).
- [74] M. Kenzelmann, S. Gerber, N. Egetenmeyer, J. L. Gavilano, Th. Strässle, A. D. Bianchi, E. Ressouche, R. Movshovich, E. D. Bauer, J. L. Sarrao, and J. D. Thompson, “Evidence for a magnetically driven superconducting Q phase of CeCoIn_5 ,” *Phys. Rev. Lett.* **104**, 127001 (2010).
- [75] G. Koutroulakis, M. D. Stewart, V. F. Mitrović, M. Horvatić, C. Berthier, G. Lapertot, and J. Flouquet, “Field evolution of coexisting superconducting and magnetic or-

- ders in CeCoIn₅,” *Phys. Rev. Lett.* **104**, 087001 (2010).
- [76] P. Schlottmann, “Lifshitz transition with interactions in high magnetic fields,” *Phys. Rev. B* **83**, 115133 (2011).
- [77] K. Momma and F. Izumi, “VESTA3 for three-dimensional visualization of crystal, volumetric and morphology data,” *J. Appl. Crystallogr.* **44**, 1272 (2011).
- [78] A. Kokalj, “XCrySDen—a new program for displaying crystalline structures and electron densities,” *J. Mol. Graph. Model.* **17**, 176 (1999).
- [79] P. Giannozzi, S. Baroni, N. Bonini, M. Calandra, R. Car, C. Cavazzoni, D. Ceresoli, G. L. Chiarotti, M. Cococcioni, I. Dabo, A. Dal Corso, S. de Gironcoli, S. Fabris, G. Fratesi, R. Gebauer, U. Gerstmann, Ch. Gougousis, A. Kokalj, M. Lazzeri, L. Martin-Samos, N. Marzari, F. Mauri, R. Mazzarello, S. Paolini, A. Pasquarello, L. Paulatto, C. Sbraccia, S. Scandolo, G. Sclauzero, A. P. Seitsonen, A. Smogunov, P. Umari, and R. M. Wentzcovitch, “QUANTUM ESPRESSO: a modular and open-source software project for quantum simulations of materials,” *J. Phys.: Condens. Matter* **21**, 395502 (2009).
- [80] P. Giannozzi, O. Andreussi, T. Brumme, O. Bunau, M. Buongiorno Nardelli, M. Calandra, R. Car, C. Cavazzoni, D. Ceresoli, M. Cococcioni, N. Colonna, I. Carnimeo, A. Dal Corso, S. de Gironcoli, P. Delugas, R. A. DiStasio, A. Ferretti, A. Floris, G. Fratesi, G. Fugallo, R. Gebauer, U. Gerstmann, F. Giustino, T. Gorni, J. Jia, M. Kawamura, H.-Y. Ko, A. Kokalj, E. Küçükbenli, M. Lazzeri, M. Marsili, N. Marzari, F. Mauri, N. L. Nguyen, H.-V. Nguyen, A. Otero de-la Roza, L. Paulatto, S. Poncé, D. Rocca, R. Sabatini, B. Santra, M. Schlipf, A. P. Seitsonen, A. Smogunov, I. Timrov, T. Thonhauser, P. Umari, N. Vast, X. Wu, and S. Baroni, “Advanced capabilities for materials modelling with Quantum ESPRESSO,” *J. Phys.: Condens. Matter* **29**, 465901 (2017).
- [81] A. Dal Corso, “Pseudopotentials periodic table: From H to Pu,” *Comput. Mater. Sci.* **95**, 337 (2014).

Supplemental Material

Electronic and dynamical properties of CeRh_2As_2 : Role of Rh_2As_2 layers and expected hidden orbital order

Andrzej Ptok,¹ Konrad J. Kapcia,² Paweł T. Jochym,¹
Jan Łażewski,¹ Andrzej M. Oleś,^{3,4} and Przemysław Piekarczyk¹

¹*Institute of Nuclear Physics, Polish Academy of Sciences, W. E. Radzikowskiego 152, PL-31342 Kraków, Poland*

²*Faculty of Physics, Adam Mickiewicz University in Poznań, Uniwersytetu Poznańskiego 2, PL-61614 Poznań, Poland*

³*Institute of Theoretical Physics, Jagiellonian University, Prof. S. Łojasiewicza 11, PL-30348 Kraków, Poland*

⁴*Max Planck Institute for Solid State Research, Heisenbergstrasse 1, D-70569 Stuttgart, Germany*

(Dated: April 23, 2021)

In this Supplemental Material we present additional results, in particular concerning:

- The details of numerical calculations in the Section below.
- Lattice constants obtained from presented *ab initio* calculations concerning Ce $4f$ electrons as valence and core electrons, respectively (in Tables S1 and S2 for the PBE pseudopotentials, and in Tables S3 and S4 for the PBEsol pseudopotentials).
- Effects of the orbital order (i.e., lowering of the system symmetry) on the phonon band structure in Fig. S1.
- The electronic density of states with orbital projections, in particular, on $4f$ states, in Fig. S2.
- The electronic band structure with the orbital projections on Rh and Ce atoms in Fig. S3.
- Comparison of the band structures in the absence and in the presence of the spin-orbit coupling for CeRh_2As_2 compound in Fig. S4.
- Comparison between the band structures of nonmagnetic CeRh_2As_2 compound and an artificial system without Ce atoms (i.e., not existing in the nature Rh_2As_2 system) in Fig. S5.
- Comparison between the band structures of the non-polarized ground state and system with fixed polarization (for CeRh_2As_2 compound) in Fig. S6.
- Modifications of the Fermi surface by the shift of the Fermi level (which corresponds to the magnetic Lifshitz transition) shown in Fig. S7.

All presented results are obtained using VASP with the $4f$ electrons of Ce atoms treated as valence electrons (except for Tables S2 and S4). Due to the fact that the PBEsol pseudopotentials correctly reproduce the experimental lattice constant, we use this pseudopotential in all calculations concerning electron and phonon properties. For additional discussion we present also the electronic band structure obtained using the QUANTUM ESPRESSO software in Fig. S8.

DETAILS OF NUMERICAL CALCULATION

The first-principles (DFT) calculations are performed using the projector augmented-wave (PAW) potentials [23] implemented in the Vienna Ab initio Simulation Package (VASP) code [18–20]. The calculations are made within generalized gradient approximation (GGA) in the Perdew, Burke, and Ernzerhof (PBE) parametrization [24] as well as a revised PBE GGA for solids (PBEsol) [25]. The summation in reciprocal space was performed over $18 \times 18 \times 8$ \mathbf{k} -point grid generated with the Monkhorst–Pack scheme [26]. The energy cutoff for the plane-wave expansion is set to 350 eV. The crystal structure as well as atom positions were optimized in the conventional unit cell with Ce $4f$ electrons treated as valence electrons. As a break condition of the optimization loop, we take energy difference of 10^{-6} eV and 10^{-7} eV for ionic and electronic degrees of freedom, respectively.

A comparison of the obtained lattice constant for the PBE and PBEsol pseudopotentials, can be found in Tables S1 and S2, and Tables S3 and S4, respectively. From the comparison with experimental data we can conclude, that the PBEsol pseudopotentials more correctly reproduce the experimental data [1]. The optimized lattice constants read

$a = 4.2216 \text{ \AA}$ and $c = 9.8565 \text{ \AA}$ and agree well with experimental data of $a = 4.2801 \text{ \AA}$ and $c = 9.8616 \text{ \AA}$ [1], respectively. Five non-equivalent atoms of the structure occupy following positions: Ce ($1/4, 1/4, 0.2528$), As ($3/4, 1/4, 0$) and ($1/4, 1/4, 0.8629$), and Rh ($3/4, 1/4, 1/2$) and ($1/4, 1/4, 0.6212$), which correspond to Wyckoff's positions $2c$, $2a$, $2c$, $2b$, and $2c$, respectively. In this case, experimentally found positions are given as: Ce ($1/4, 1/4, 0.25469$), As ($3/4, 1/4, 0$) and ($1/4, 1/4, 0.86407$), and Rh ($3/4, 1/4, 1/2$) and ($1/4, 1/4, 0.61742$) [1].

The electronic band structures are also evaluated within the QUANTUM ESPRESSO [79, 80]. In this case, during calculations we use pseudopotentials developed in a frame of PSLIBRARY [81]. Additionally, we use the cutoff for charge density and wave function with the nominal value increased by 100 Ry. However, due to different electronic configuration of the Ce atoms (i.e., $[\text{Xe}] 6s^2 4f^{1/2} 5d^{3/2}$) than in the case of VASP calculations, the positions of the $4f$ states of Ce atoms can be overestimated – cf. Fig. S8. Here, we should notice that the electronic band structure obtained within the full-potential linearized augmented planewave method by the WIEN2K software (see Ref. [67]) is similar to this obtained from VASP.

Phonon calculations were performed in the supercell with 40 atoms containing $2 \times 2 \times 1$ conventional unit cells. The phonon dispersion curves and phonon density of states (DOS) are calculated using ALAMODE software [21]. Calculations are performed for the thermal distribution of multi-displacements of atoms at $T = 50 \text{ K}$, generated within HECSS procedure [22]. Energy of the one hundred different configurations of the supercells and the Hellmann-Feynman forces acting on all atoms are determined using VASP. In calculated dynamical properties, we include contributions from harmonic and cubic interatomic force constants to phonon frequencies.

TABLE S1. Experimental (taken from Ref. [1]) and theoretical (*ab initio*) lattice constants obtained in the absence of magnetism (NM), assuming antiferromagnetic (AFM) order (in two directions), and assuming ferromagnetic (FM) order (in two directions) as initial magnetic orders. During calculations, the final states conserved assumed magnetic orders (AFM and FM with final magnetic moments $0.27 \mu_B$ and $0.10 \mu_B$ at Ce atoms, respectively). In contrary to this, calculations starting from the NM state (all magnetic moments equal zero) lead finally to small magnetic moments with magnitude smaller than $0.03 \mu_B$. For the theoretical results we show also δE , denoting the difference of energy between ground state (GS) and given magnetic order. Results obtained with PBE pseudopotential treatment of $4f$ electrons of Ce atoms as valence electrons and in the presence of the spin-orbit coupling.

	exp. [1]	NM	AFM		FM	
		—	$M ab$	$M c$	$M ab$	$M c$
δE (meV)	—	(GS) 0.000	3.135	4.082	4.447	4.606
a (Å)	4.2801	4.2802	4.2804	4.2802	4.2800	4.2798
c (Å)	9.8616	9.9752	9.9788	9.9773	9.9761	9.9766

TABLE S2. The same as in Table S1, but from *ab initio* calculations with PBE pseudopotential treatment of $4f$ electrons of Ce atoms as core electrons. Independently of the initial magnetic moments configurations, the final states do not exhibit any finite magnetic moments.

	exp. [1]	NM	AFM		FM	
		—	$M ab$	$M c$	$M ab$	$M c$
δE (meV)	—	0.108	0.112	0.116	(GS) 0.000	0.047
a (Å)	4.2801	4.3243	4.3243	4.3243	4.3243	4.3243
c (Å)	9.8616	10.0442	10.0442	10.0442	10.0442	10.0442

TABLE S3. The same as in Table S1, but in the case of PBEsol pseudopotentials (i.e., $4f$ electrons of Ce atoms treated as valence electrons).

	exp. [1]	NM	AFM		FM	
		—	$M ab$	$M c$	$M ab$	$M c$
δE (meV)	—	0.260	(GS) 0.000	0.078	0.148	0.160
a (Å)	4.2801	4.2214	4.2216	4.2215	4.2215	4.2214
c (Å)	9.8616	9.8560	9.8565	9.8561	9.8562	9.8562

TABLE S4. The same as in Table S2, but in the case of PBEsol pseudopotentials (i.e., $4f$ electrons of Ce atoms treated as core electrons).

	exp. [1]	NM	AFM		FM	
		—	$M ab$	$M c$	$M ab$	$M c$
δE (meV)	—	0.002	(GS) 0.000	6.255	0.002	0.000
a (Å)	4.2801	4.2670	4.2670	4.2666	4.2669	4.2669
c (Å)	9.8616	9.9224	9.9224	9.9225	9.9227	9.9227

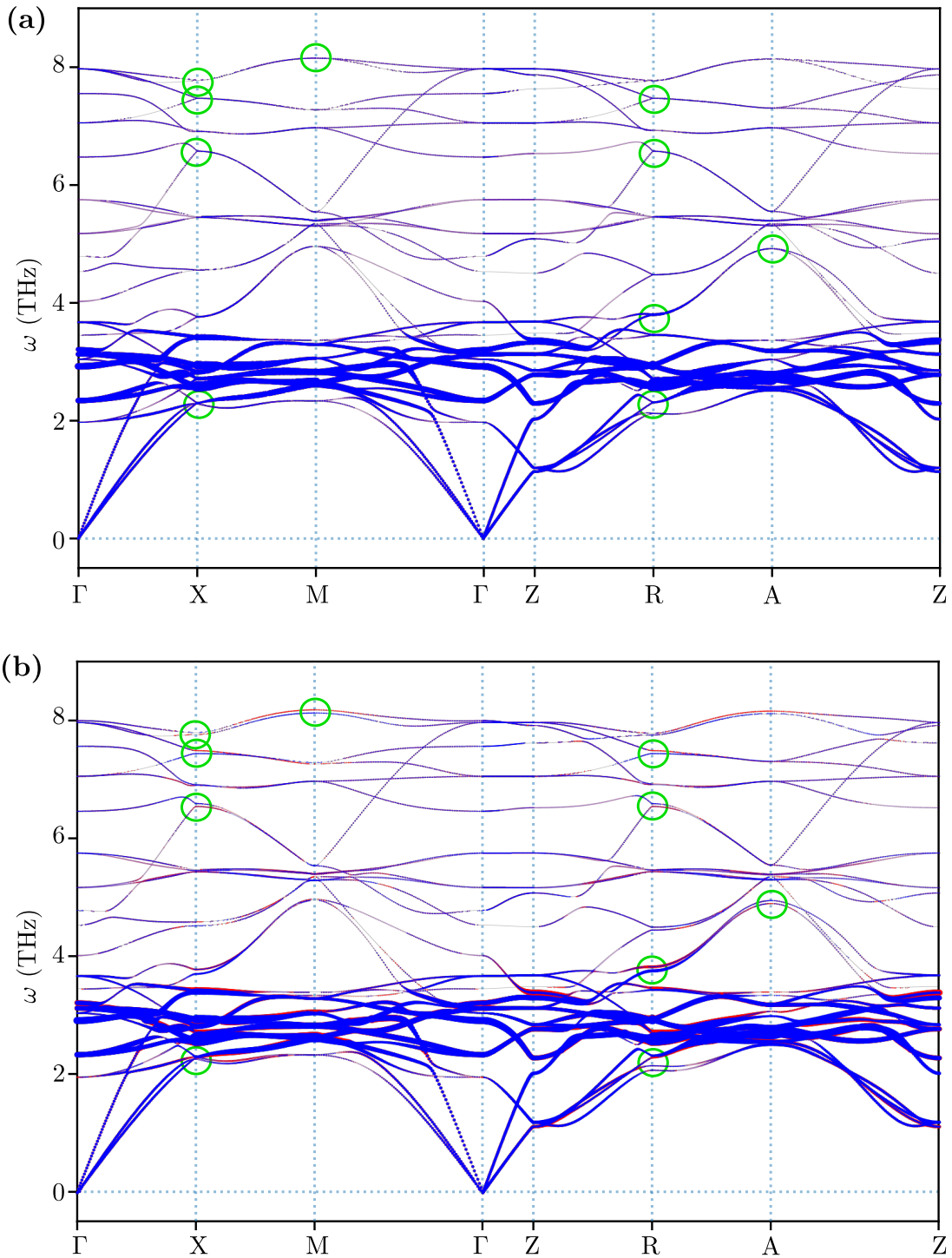


FIG. S1. Effects of hidden orbital order on the phonon spectra—shown by width and color of line corresponding to the projection of the polarization vector on the 1^{st} and 2^{nd} Ce atoms. In the case of two non-distinguishable Ce atoms the $P4/nmm$ symmetry exists. Introduction of the orbital order leads to the realization of two sub-lattices, distinguishable by realized pseudo-orbitals at Ce atoms. A main role on the realization of this orbital order is played by two non-equivalent Rh_2As_2 planes surrounding Ce atoms from top and bottom. Assuming $P4/nmm$ symmetry (a), the phonon projection on the 1^{st} and 2^{nd} Ce atoms (red and blue color, respectively), are non-distinguishable (system is described by 64 symmetry operations). Introduction of orbital order leads to the lowering of the system symmetry to $P4mm$ symmetry (b). In this case system undergoes only a half of symmetry operations, i.e., 32 operations. This is well visible by projection of polarization vectors on the 1^{st} and 2^{nd} Ce atoms in a form of splitting red and blue lines. From this, degeneracy of the band structure in high symmetry points are lifted [e.g., cf. green circles at (a) and (b)]. This effect is similar to observed in electronic band structure, e.g. as the emergence of the Dirac semi-metals after introducing magnetic order. Both results were obtained from the same dataset of hundred multidisplacement configurations corresponding to 50 K. Results for PBEsol pseudopotentials in the presence of SOC and with $4f$ electrons of Ce atoms treated as valence electrons.

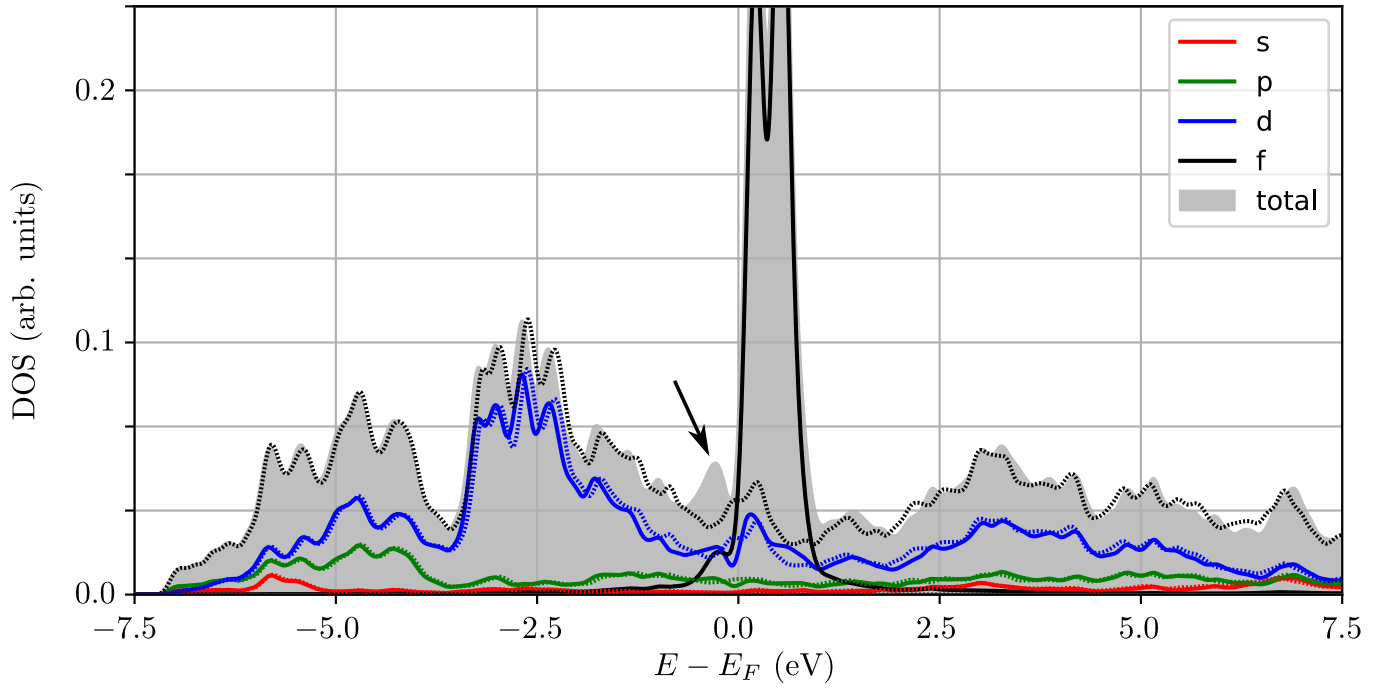


FIG. S2. Orbital projected electronic DOS in the presence of SOC. Solid and dashed lines (colors as labeled) correspond to different treatments of the $4f$ electrons originating from Ce atoms (as valence and core electrons, respectively). Dashed black line corresponds to the total DOS in the case of Ce $4f$ electrons treated as core electrons, whereas the grey background denotes the total DOS for the case of Ce $4f$ electrons treated as valence electrons. The modification due to f - d orbital hybridization is observed around the Fermi level (marked by black arrow). Results for PBEsol pseudopotentials.

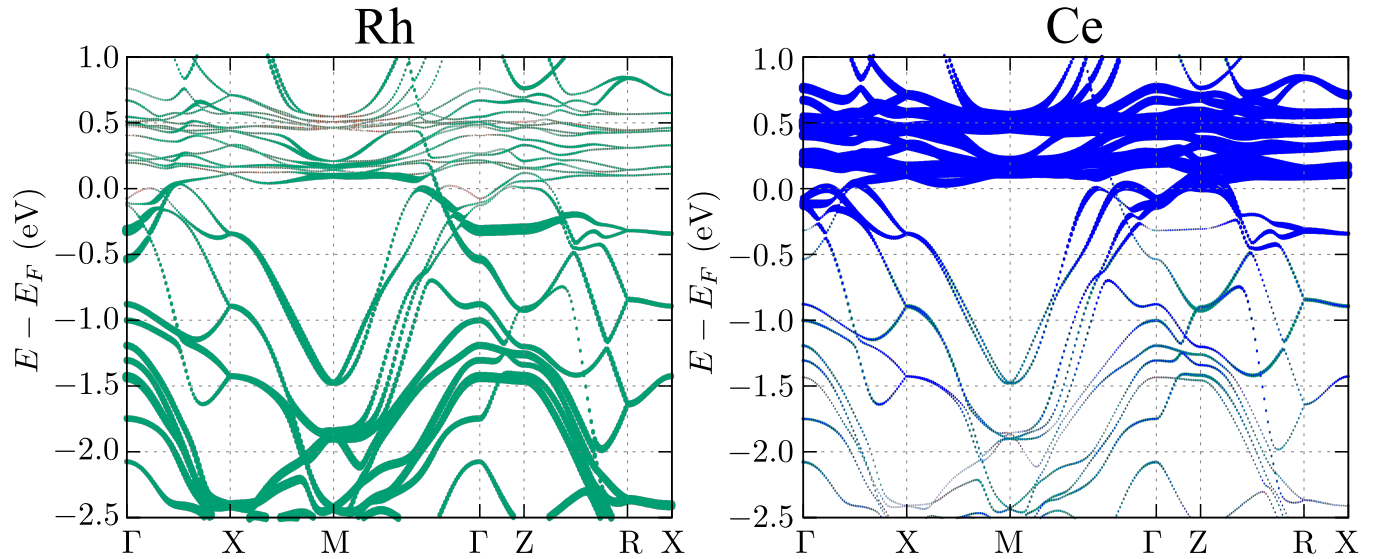


FIG. S3. Orbital projected electronic band structure for Rh and Ce atoms (left and right panels, respectively). Red, green, and blue color correspond to p , d , and f orbitals, respectively. Sizes of dots correspond to the value of the contribution of a given orbital. Results for PBEsol pseudopotentials in the presence of SOC and with $4f$ electrons of Ce atoms treated as valence electrons.

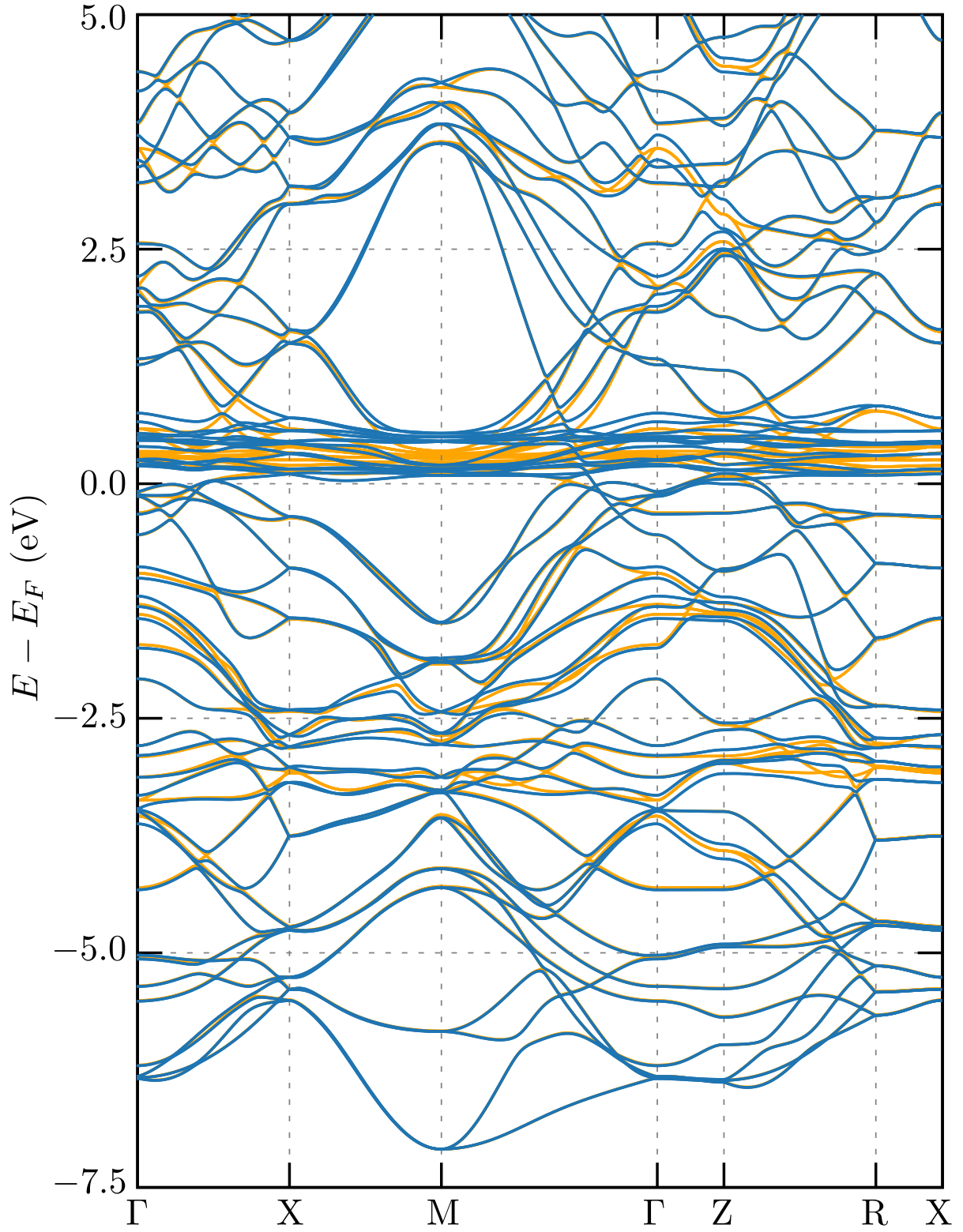


FIG. S4. Comparison between the electronic band structures of the non-magnetic ground state of CeRh₂As₂ in the absence and in the presence of SOC (solid orange and blue lines, respectively). Results for PBEsol pseudopotentials with 4*f* electrons of Ce atoms treated as valence electrons.

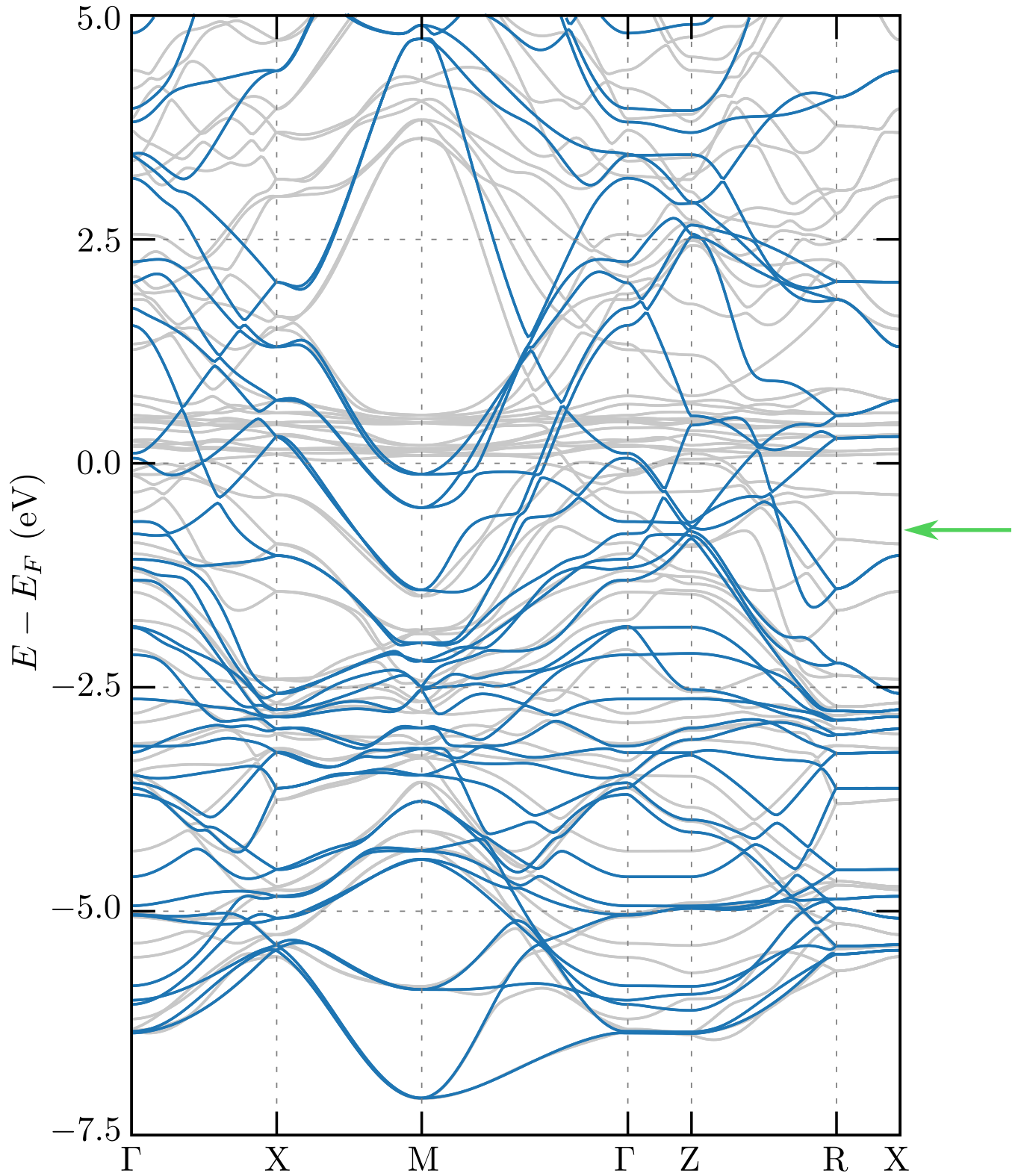


FIG. S5. Comparison between the electronic band structures of the non-magnetic ground state of CeRh_2As_2 (solid gray lines) and an artificial structure without Ce atoms (blue solid lines). Zero-energy denotes the Fermi level of CeRh_2As_2 . Green arrow (on the right) show the location of Fermi level for the artificial system. Results obtained in the presence of spin-orbit coupling. Results for PBEsol pseudopotentials in the presence of SOC and with $4f$ electrons of Ce atoms treated as valence electrons.

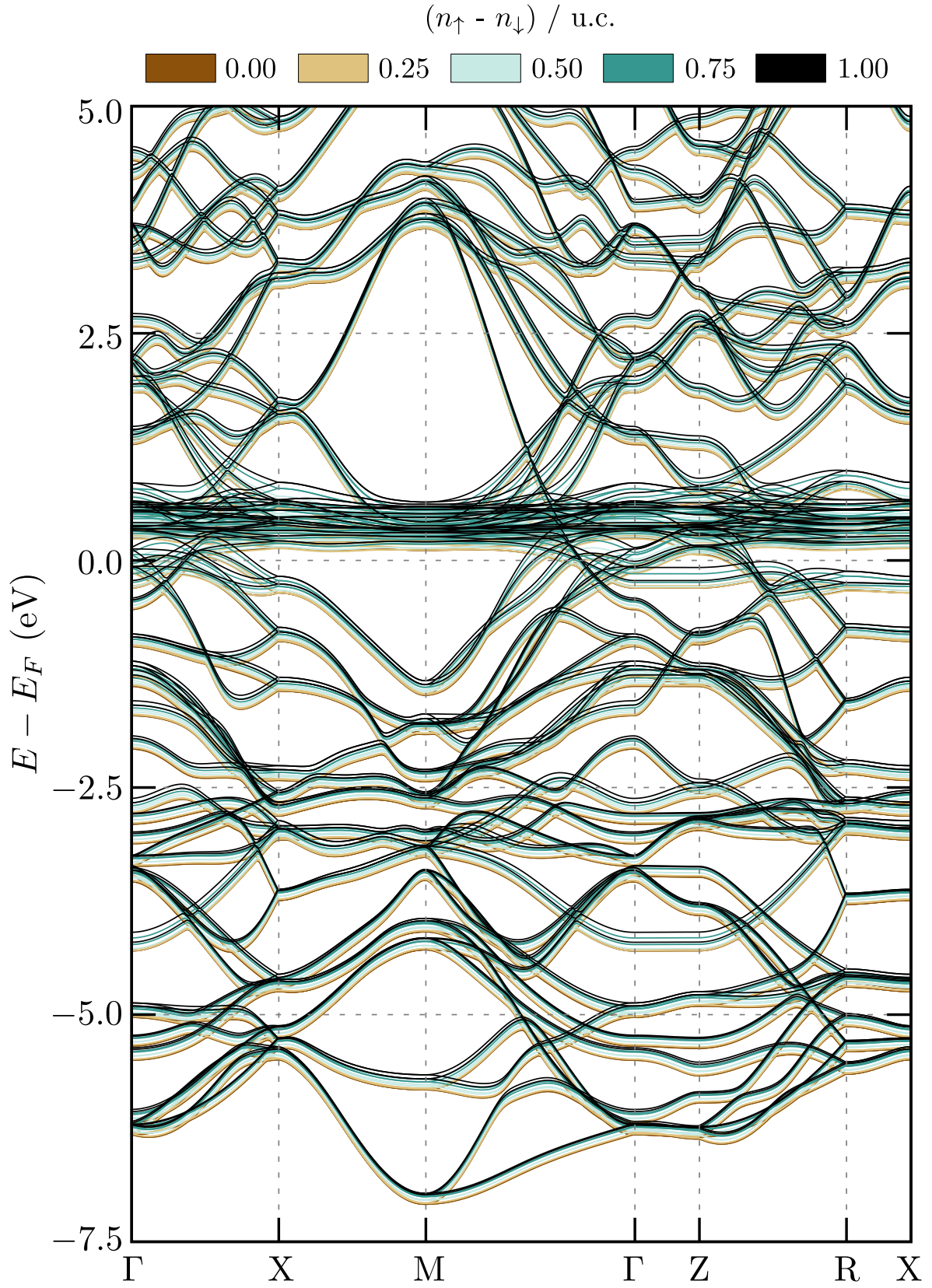


FIG. S6. Comparison between the electronic band structures between the non-magnetic ground state (i.e., in the absence of magnetic polarization; solid gray lines) and nonphysically polarized state (difference between electrons with opposite spins per the conventional unit cell is equal as labeled; dispersion curves for spin-up and spin-down electrons are shown by solid red and blue lines respectively). Results obtained in the absence of the spin-orbit coupling for CeRh_2As_2 . Results for PBEsol pseudopotentials in the absence of the SOC and with $4f$ electrons of Ce atoms treated as valence electrons.

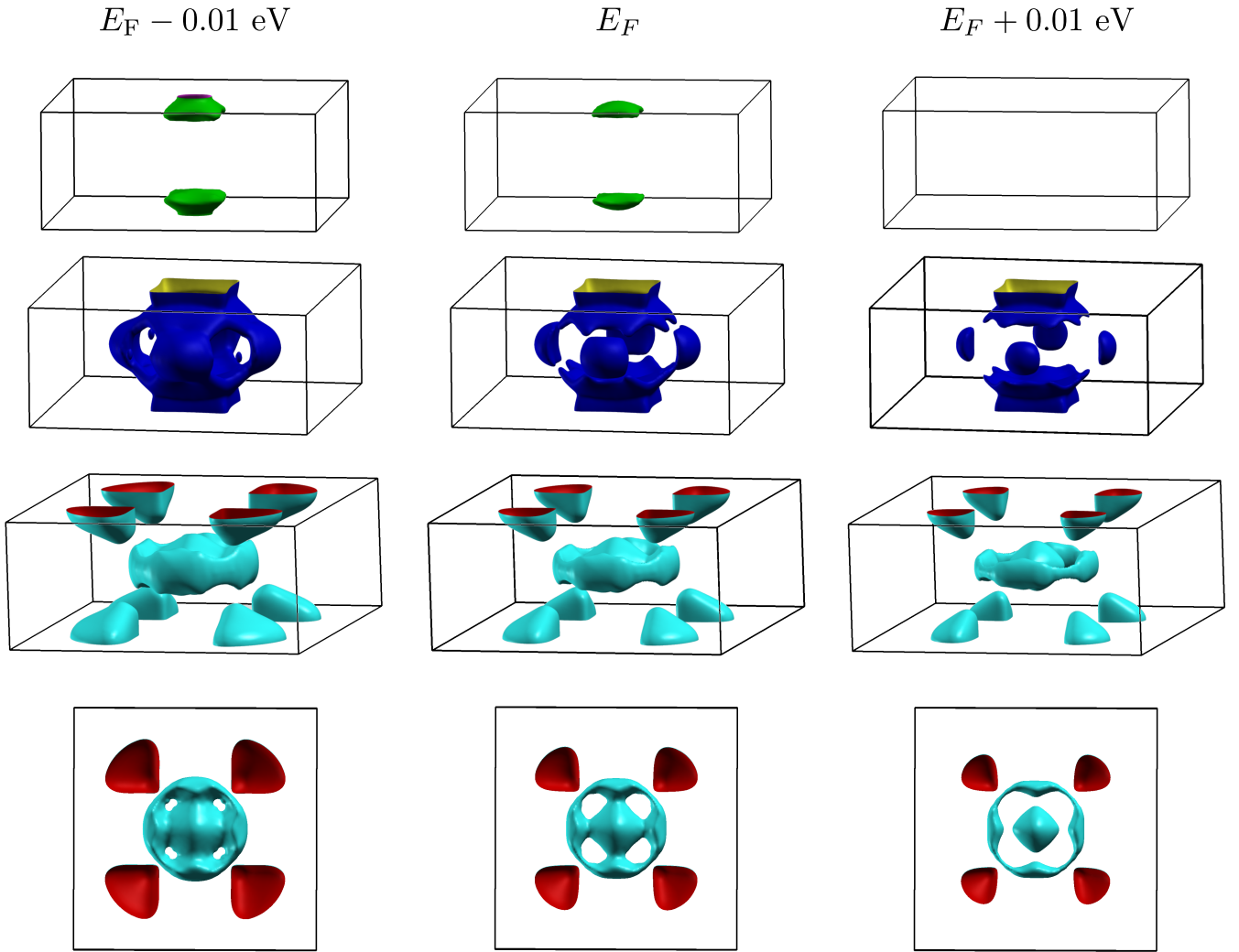


FIG. S7. Modification of the Fermi surface by shifting the Fermi level (as labeled), what corresponds to the realization of the magnetic Lifshitz transition. Increasing magnetic field leads to lift spin degeneracy and splitting of the bands. During this process, the modification of the Fermi surface shape can be observed. In the extreme case (top panels) the Fermi pocket can change its shape (left top panel) or totally disappear (right top panel). First three rows correspond to different pockets of the Fermi surface, whereas the bottom row shows the view from the top of the pocket shown in third row. Results for PBEsol pseudopotentials in the presence of SOC and with $4f$ electrons of Ce atoms treated as valence electrons.

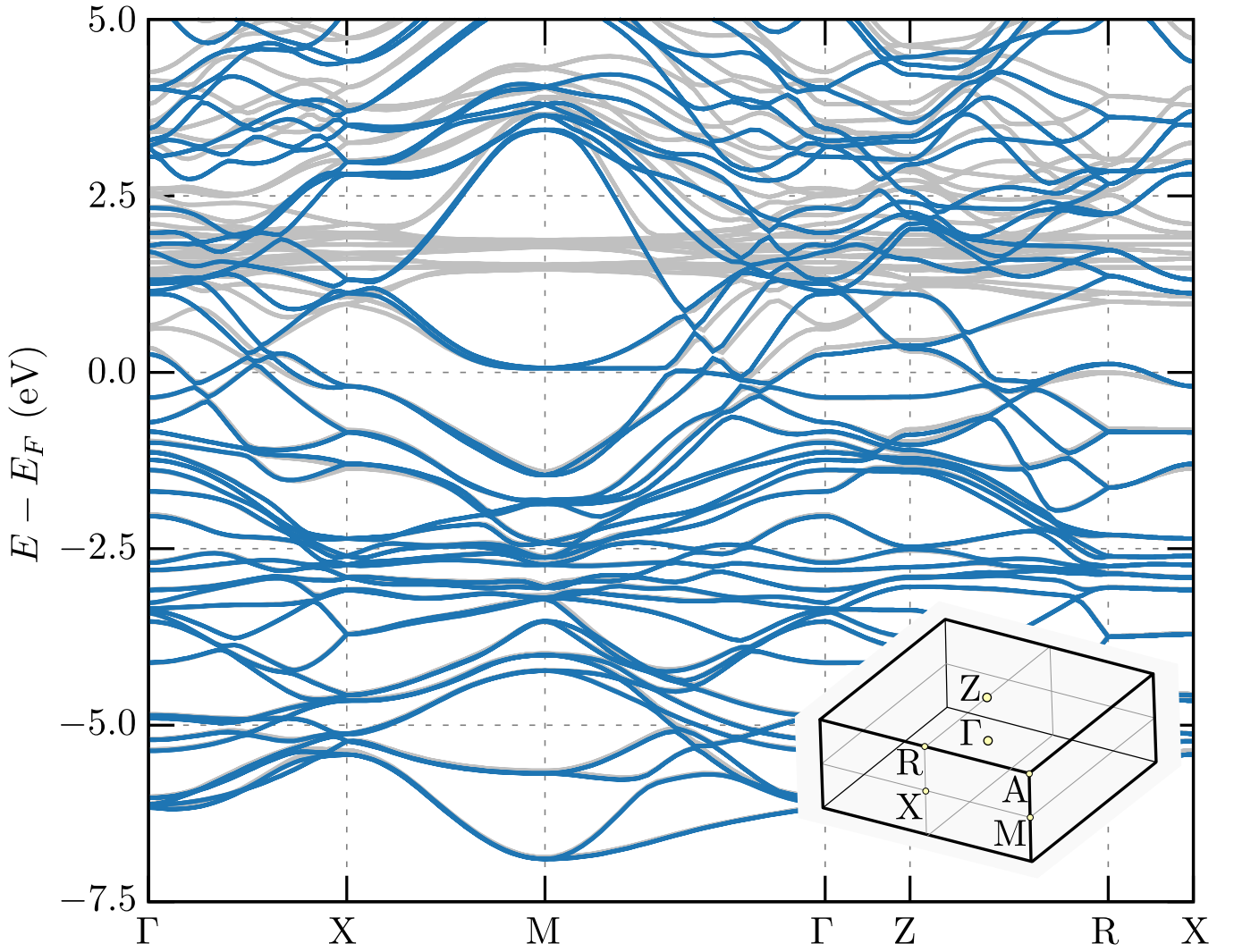


FIG. S8. Electronic band structures in the presence of the spin-orbit interaction obtained within the QUANTUM ESPRESSO software. In this calculations, the PSLIBRARY pseudopotentials were used. Solid blue and gray lines correspond to different treatments of the Ce $4f$ electrons (as core and valence electrons, respectively). Due to different electronic configuration of the Ce atoms (i.e., $[\text{Xe}] 6s^2 4f^{1/2} 5d^{3/2}$) than in the VASP pseudopotentials (i.e., $[\text{Xe}] 6s^2 4f^1 5d^1$) the positions of the $4f$ electron bands can be overestimated.